JM PAPERS

Multifractality and scale-free network topology in a noise-perturbed laminar jet

Yu Guan[1,2,†], Yuanhang Zhu[2,3], Zhijian Yang[2], Bo Yin[2], Vikrant Gupta[4,5] and Larry K.B. Li[2,6,†]

[1]Department of Aeronautical and Aviation Engineering, The Hong Kong Polytechnic University, Kowloon, Hong Kong

[2]Department of Mechanical and Aerospace Engineering, The Hong Kong University of Science and Technology, Clear Water Bay, Hong Kong

[3]Department of Mechanical and Aerospace Engineering, University of Virginia, Charlottesville, VA 22904, USA

[4]Guangdong Provincial Key Laboratory of Turbulence Research and Applications, Department of Mechanics and Aerospace Engineering, Southern University of Science and Technology, Shenzhen, PR China

[5]Guangdong-Hong Kong-Macao Joint Laboratory for Data-Driven Fluid Mechanics and Engineering Applications, Southern University of Science and Technology, Shenzhen, PR China

[6]Guangdong–Hong Kong–Macao Joint Laboratory for Data-Driven Fluid Mechanics and Engineering Applications, The Hong Kong University of Science and Technology, Clear Water Bay, Hong Kong

We present experimental evidence of multifractality and scale-free network topology in a noise-perturbed laminar jet operated in a globally stable regime, prior to the critical point of a supercritical Hopf bifurcation and prior to the saddle-node point of a subcritical Hopf bifurcation. For both types of bifurcation, we find that (i) the degree of multifractality peaks at intermediate noise intensities, (ii) the conditions for peak multifractality produce a complex network whose node degree distribution obeys an inverse power-law scaling with an exponent of $2 < \gamma < 3$, indicating scale-free topology and (iii) the Hurst exponent and the global clustering coefficient can serve as early warning indicators of global instability under specific operating and forcing conditions. By characterising the noise-induced dynamics of a canonical shear flow, we demonstrate that the multifractal and scale-free network dynamics commonly observed in turbulent flows can also be observed in laminar flows under certain stochastic forcing conditions.

Key words: instability, jets, nonlinear dynamical systems

† Email addresses for correspondence: yu.guan@polyu.edu.hk, larryli@ust.hk

972 A6-1

1. Introduction

Above a critical Reynolds number, a low-density jet can become globally unstable, transitioning from a spatial amplifier of extrinsic disturbances to a self-excited oscillator with intrinsic dynamics prescribed by a wavemaker (Chomaz, Huerre & Redekopp 1988; Lesshafft & Marquet 2010; Coenen *et al.* 2017; Chakravarthy, Lesshafft & Huerre 2018). This transition can be viewed as a Hopf bifurcation from a fixed point perturbed by noise to a limit cycle associated with nonlinear global oscillations (Huerre & Monkewitz 1990; Kyle & Sreenivasan 1993; Hallberg & Strykowski 2006; Li & Juniper 2013*b*; Kushwaha *et al.* 2022). Such oscillations can be useful in some processes (e.g. enhancing mixing in combustion systems) but they can be damaging in other processes (e.g. triggering vibrations in aeroelastic systems). There is thus a need to develop early warning indicators of global instability so that preemptive action can be taken.

Noise exists in nearly all real systems but does not always act to obscure the deterministic dynamics. For example, noise-induced phenomena, such as coherence resonance, stochastic resonance and noise-induced synchronisation, can sometimes be used to predict and control the stability and dynamics of nonlinear excitable systems (Pikovsky, Rosenblum & Kurths 2003; Lindner *et al.* 2004; Scheffer *et al.* 2009; Lee *et al.* 2020). This has been demonstrated in various systems ranging from optically trapped atoms (Wilkowski *et al.* 2000) to schools of fish (Jhawar *et al.* 2020) to chemically reacting/non-reacting flows (Noiray & Schuermans 2013; Lee *et al.* 2021; Sieber, Paschereit & Oberleithner 2021). However, most studies involving fluids have focused on turbulent flows. In the present study, we show for the first time that stochastically forcing a laminar flow can cause it to exhibit the same type of multifractal and scale-free network dynamics commonly seen in turbulent flows. From this, we conclude that even when globally stable, a noise-perturbed laminar jet can behave in ways more complex than just a noisy fixed point, leading to fresh opportunities for the development of global instability precursors.

1.1. *Multifractality in flow systems*

Data collected from a complex system typically contain a wide range of spatial and temporal scales due to the nonlinear interactions among the various subcomponents (Coniglio, De Arcangelis & Herrmann 1989). Such data are often self-similar, with fluctuations obeying fractal scaling, sometimes across multiple orders of magnitude (Kantelhardt 2012). If the dynamics can be captured with a single exponent (the fractal dimension), then the data are monofractal. If a continuous spectrum of exponents (the singularity spectrum) is required, however, then the data are multifractal. Thus, the fluctuations of a multifractal signal obey different scaling laws at different amplitudes. Such behaviour has been widely observed in turbulence (Sreenivasan 1991). In seminal experiments, Meneveau & Sreenivasan (1991) showed that the multiplicative processes governing turbulent energy dissipation have a multifractal signature. Flohr & Olivari (1994) analysed the passive scalar field of a turbulent jet and found a multifractal spectrum. López *et al.* (2017) performed a similar analysis on a turbulent plume and found that its spatiotemporal evolution can be described by multifractal metrics such as the width and symmetry of the singularity spectrum. Viggiano *et al.* (2021) examined the dynamics of a variable-density jet in the laminar, transitional and turbulent regimes. They found that the degree of multifractality peaks at a transitional Reynolds number, close to the turbulent threshold. From these and other studies, there is now compelling evidence that multifractality is a characteristic feature of turbulent flows. However, to the best of the

authors' knowledge, multifractality has yet to be observed in a laminar flow, despite its potential role in the development of early warning indicators of self-excited flow oscillations (Nair & Sujith 2014; Sujith & Pawar 2021).

1.2. *Scale-free networks in flow systems*

Network analysis provides a versatile framework within which to analyse the connectivity patterns of a complex system (Iacobello, Ridolfi & Scarsoglio 2021). Many network properties (e.g. connectivities and scalings) are universal, appearing in many different flow systems (Taira & Nair 2022). One such property is an inverse power-law scaling in the node degree distribution, the defining feature of a scale-free network (Barabási & Albert 1999). Specifically, in a scale-free network, the fraction of nodes with k edges to other nodes scales asymptotically as $P(k) \sim k^{-\gamma}$, with $2 < \gamma < 3$. This power-law scaling is thought to arise from two mechanisms: nodal growth and preferential attachment (Barabási & Albert 1999).

Scale-free networks are ubiquitous in turbulence. For example, Liu, Zhou & Yuan (2010) found scale-free topology in complex networks built from time traces of the energy dissipation rate in three-dimensional fully developed turbulence. Taira, Nair & Brunton (2016) showed that the vortical interactions in two-dimensional decaying isotropic turbulence can be represented as a scale-free network. They also showed that the network is only weakly sensitive to random forcing but is strongly sensitive to forcing directed at the network hubs (vortical structures). Turning to reacting flows, Murugesan & Sujith (2015) used the visibility algorithm to build complex networks from pressure signals measured in a turbulent premixed combustor during its transition from a low-amplitude aperiodic state (combustion noise) to a high-amplitude limit-cycle state (thermoacoustic instability). They found that the former state is characterised by a scale-free network, whose topology becomes ordered at the onset of thermoacoustic instability. Shortly after, this loss of scale-free behaviour was used by Murugesan & Sujith (2016) as an instability precursor. Like multifractality (§ 1.1), scale-free network topology has been observed only in turbulent flows, leaving many open questions about its potential existence in laminar flows and whether its destruction can be utilised as a precursor of global instability.

1.3. *Contributions of the present study*

We aim to answer three research questions. (i) Can the multifractal and scale-free network dynamics commonly seen in turbulent flows ever be seen in laminar flows? (ii) If so, under what specific operating and forcing conditions? (iii) Can changes in multifractality and scale-free network topology be used to forewarn of an impending critical transition, such as a supercritical or subcritical Hopf bifurcation to a global mode?

To answer those questions, we perform laboratory experiments on a prototypical hydrodynamic oscillator: a low-density inertial laminar jet. We examine the jet as it transitions from a globally stable to globally unstable state via a supercritical or subcritical Hopf bifurcation. By stochastically forcing the jet in the globally stable state, we find that the noise-induced dynamics of this laminar flow can resemble the inherent dynamics of turbulent flows, with regard to multifractality and scale-free network topology. We then show how the loss of these two features en route to a Hopf bifurcation can be used for early detection of global instability, under specific operating and forcing conditions.

2. Experimental set-up

The experimental set-up is identical to that used in our previous work on the noise-induced dynamics and system identification of low-density jets (Zhu, Gupta & Li 2017; Lee *et al.* 2019; Zhu, Gupta & Li 2019). The set-up features a round convergent nozzle with an exit diameter of $D = 6$ mm and an area contraction ratio of 100:1. Upstream of the nozzle is a settling chamber containing mesh screens and honeycomb sections as flow conditioners. To set the jet density ratio ($S \equiv \rho_j/\rho_\infty$), we mix gaseous helium and air at flow rates specified by mass flow controllers. Previous work by Zhu *et al.* (2017) on low-density jets in the incompressible momentum-dominated regime has shown that S is a key parameter controlling whether a supercritical or subcritical Hopf bifurcation occurs with increases in the transverse curvature or the Reynolds number, $Re \equiv \rho_j U_j D/\mu_j$, where U_j is the centreline flow velocity and μ_j is the dynamic viscosity of the jet fluid. We expose the jet to external stochastic forcing, in the form of broadband acoustic waves generated by a loudspeaker mounted at the bottom of the settling chamber. The loudspeaker is driven by a white Gaussian noise signal (0–20 MHz bandwidth) produced by a function generator (Keysight 33512B). We measure the jet response with a precalibrated single-normal hot-wire probe (DANTEC 55P16) positioned at $(x/D, r/D) = (1.5, 0)$, where x and r are the streamwise and radial coordinates, respectively. This sensor location is within the jet potential core, where the wavemaker resides and where the jet fluid concentration remains constant, facilitating conversion of the hot-wire voltage (Li & Juniper 2013*a*). We sample the hot-wire voltage at 32 768 Hz for 8 s using a 16-bit analogue-to-digital converter (NI USB-6212), capturing time traces of the local streamwise velocity, $u(t)$. We define the noise intensity as the root-mean-square velocity fluctuation normalised by the time-averaged velocity, $\sigma \equiv u'_{0,rms}/\bar{u}_0$, where the subscript 0 denotes measurements taken at the nozzle exit centreline, $(x/D, r/D) = (0, 0)$. Further details on the experimental set-up and measurement procedure can be found in our previous work (Zhu *et al.* 2017; Lee *et al.* 2019; Zhu *et al.* 2019).

3. Results and discussion

3.1. *Overview of the jet dynamics*

We first consider the unforced jet dynamics. Figure 1 shows the bifurcation diagrams for a supercritical case ($S = 0.14$) and a subcritical case ($S = 0.18$), both with the forward path (increasing Re) and the backward path (decreasing Re) shown together. In the supercritical case (figure 1*a*), the two paths overlap, with a shared Hopf point ($Re = 590$). In the subcritical case (figure 1*b*), the two paths do not overlap because a hysteretic bistable regime exists between the saddle-node point ($Re = 760$) and the Hopf point ($Re = 785$).

In the sections on multifractality (§ 3.2) and scale-free network topology (§ 3.3), we apply stochastic forcing at the Hopf point itself in the supercritical case (figure 1*a*: $Re = 590$) and near the saddle-node point in the subcritical case (figure 1*b*: $Re = 755$). We choose these specific operating points for noise application because they are at the edge of the unconditionally globally stable regime (Zhu *et al.* 2019). In the sections on early detection of global instability (§ 3.4) and the universal scaling between fractal-based and coherence-based precursors (§ 3.5), we apply stochastic forcing at every operating point, including before and after the Hopf and saddle-node points as well as at those points themselves. However, in every section of this paper, we also examine cases where stochastic forcing is not applied at all; in these cases, the jet is subjected only to its inherent background noise.
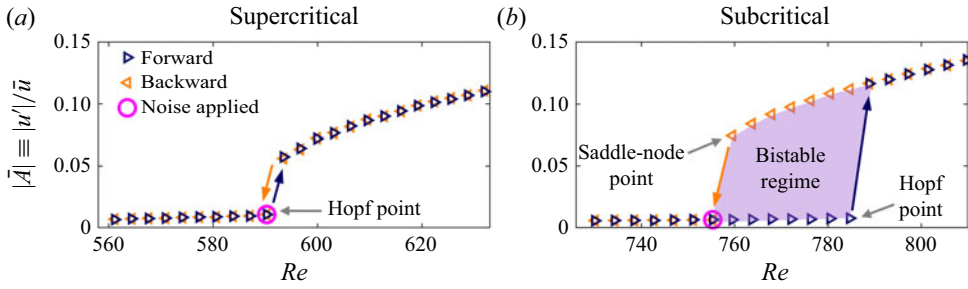
Figure 1. Bifurcation diagrams of the jet undergoing (*a*) a supercritical Hopf bifurcation with $S = 0.14$ and (*b*) a subcritical Hopf bifurcation with $S = 0.18$. In §§ 3.2 and 3.3, stochastic forcing is applied at the Hopf point itself in the supercritical case ($Re = 590$) and near the saddle-node point in the subcritical case ($Re = 755$). In §§ 3.4 and 3.5, stochastic forcing is applied at all the operating points shown.

3.2. *Multifractality*

We perform a multifractal detrended fluctuation analysis to characterise the fractal and multifractal properties of the temporal fluctuations in the jet velocity signal $u(t)$. As noted by Kantelhardt *et al.* (2002), this involves computing the qth-order fluctuation function:

$$F_q \equiv \left(1/n \sum_{i=1}^{n} \left[1/w \sum_{t=1}^{w} [y_i'(t) - \mathbb{Y}_i]^2 \right]^{q/2} \right)^{1/q}, \qquad (3.1)$$

where $y_i'(t)$ consists of n non-overlapping segments of equal width w extracted from the cumulative deviate series, $y_j' \equiv \sum_{t=1}^{j} [u(t) - \bar{u}]$ with $j = 1, 2, \ldots, N$ and $N = nw$ being the total length of $u(t)$. For the 0th-order moment ($q = 0$), the fluctuation function is defined as

$$F_0 \equiv \exp \left(1/2n \sum_{i=1}^{n} \log \left[1/w \sum_{t=1}^{w} [y_i'(t) - \mathbb{Y}_i]^2 \right] \right). \qquad (3.2)$$

For all q, we detrend each data segment by subtracting a local linear fit $\mathbb{Y}_i$ from $y_i'(t)$ itself. The power-law scaling exponent in $F_q \sim w^{H_q}$ is known as the generalised Hurst exponent. The Hurst exponent at $q = 2$, or H_2, is commonly used to characterise the long-range dependence of a time series (Hurst 1951; Kantelhardt *et al.* 2002). In figure 2(*a*,*b*), we demonstrate how H_2 can be extracted from the log–log plot of F_2 and w via the local slope in the linear scaling regime ($2^7 \leqslant w \leqslant 2^{11}$), as per the recommendations of Ihlen (2012).

We find that increasing σ leads to a decrease in H_2 for both types of bifurcation. In the supercritical case (figure 2*c*), H_2 remains below 0.5 for all values of σ, indicating that the jet dynamics are always anti-persistent, dominated by mean reversion processes that return future values of the signal to the long-term average (Hurst 1951). This antipersistence arises even at the lowest possible value of σ in our experimental facility ($\sigma = 1.77 \times 10^{-3}$), which corresponds to the inherent background noise in the jet at the supercritical Hopf point ($Re = 590$) without any external stochastic forcing.

In the subcritical case (figure 2*d*), H_2 is initially greater than 0.5 for low values of σ, indicating that the jet dynamics are persistent, dominated by long-memory trending processes that cause future values of the signal to follow its previous values (Hurst 1951). However, as σ increases, H_2 falls below 0.5, indicating antipersistence. This transition
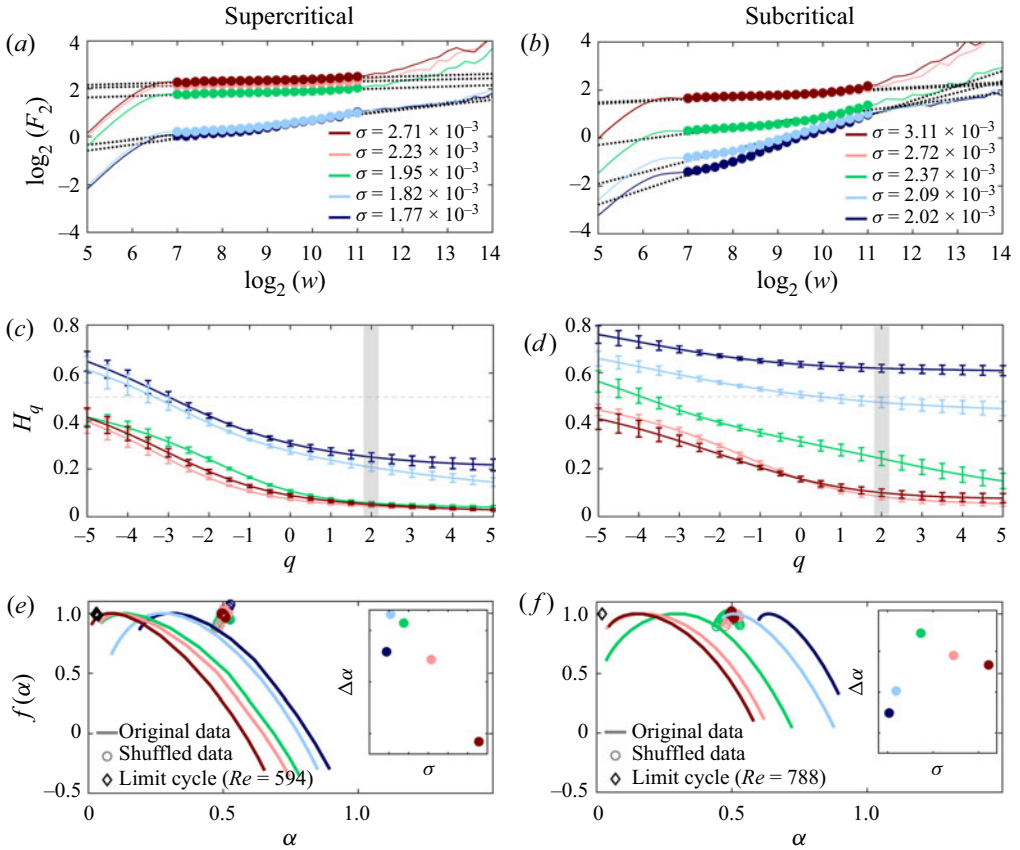
Figure 2. (*a,b*) Fluctuation function F_2 vs the segment width w on a log–log plot, (*c,d*) the generalised Hurst exponent H_q, and (*e,f*) the singularity spectrum, all at different values of σ. The supercritical and subcritical cases are shown in the left and right columns, respectively. In panels (*a,b*), the bolded markers denote the data used to compute H_2. In panels (*c,d*), the error bars are the 90 % confidence intervals.

from persistence ($H_2 > 0.5$) to antipersistence ($H_2 < 0.5$) occurs only in the subcritical case and can be explained as follows. When σ is low, the forcing is weak, and linear response theory holds. Because the operating point in the subcritical case is relatively far from the Hopf point (see the magenta marker in figure 1*b*), the weak forcing cannot perturb the jet significantly away from its stable fixed point, resulting in dynamics that are persistently dominated by the fixed point itself. When σ is high, however, the forcing is strong enough to intermittently perturb the jet away from the stable fixed point and towards the basin of attraction of an unstable limit cycle, producing dynamics with signatures of both of these attractors and thus leading to antipersistence. In the supercritical case (figure 2*c*), a similar transition from persistence to antipersistence is not observed because the operating point is so close to the Hopf point (figure 1*a*) that the jet becomes marginally globally unstable (Huerre & Monkewitz 1990), with even inherent background noise being sufficient to cause antipersistent dynamics via coherence resonance (Zhu *et al.* 2019).

Figure 2(*c,d*) shows that, for both types of bifurcation and regardless of σ, H_q varies with q, indicating that the low- and high-amplitude fluctuations in $u(t)$ scale differently (Kantelhardt *et al.* 2002). This evidence of multifractality appears even when the jet is subjected only to its inherent background noise, without any external forcing. In the

972 A6-6

supercritical case, at both low and high noise intensities (figure 2c: $\sigma = 1.77 \times 10^{-3}$ and $\geqslant 1.95 \times 10^{-3}$), H_q levels off at high positive q, indicating that the multifractal structures are dominated by low-amplitude fluctuations (Ihlen 2012). Crucially, at an intermediate noise intensity (figure 2c: $\sigma = 1.82 \times 10^{-3}$), H_q does not level off, indicating that the multifractal structures consist of both low- and high-amplitude fluctuations, although the former remain dominant. Thus, the multifractal characteristics of this jet depend strongly on the noise intensity: only at an intermediate noise intensity can strong multifractal structures emerge. Similar findings hold for the subcritical case (figure 2d), where the critical noise intensity is $\sigma = 2.37 \times 10^{-3}$.

Figure 2(e,f) shows the singularity spectrum, as computed via the Legendre transform with a qth-order mass exponent of $\tau_q = qH_q - 1$, a singularity (Hölder) exponent of $\alpha = \partial \tau_q / \partial q$ and a singularity dimension of $f(\alpha) = q\alpha - \tau_q$. For both types of bifurcation and regardless of σ, we find that the singularity spectrum is distributed along an inverted parabolic arc of appreciable width ($\Delta\alpha \equiv \alpha_{max} - \alpha_{min}$), confirming the presence of multifractality. If the signal were simply monofractal, the singularity spectrum would cluster at a discrete point (Kantelhardt *et al.* 2002). The spectral width $\Delta\alpha$ is thus a measure of the range of scales present in the signal, i.e. the degree of multifractality (Silchenko & Hu 2001; Ihlen 2012). We find that $\Delta\alpha$ increases, peaks and then decreases as σ increases (figure 2e,f insets), implying that the degree of multifractality reaches a maximum at intermediate noise intensities: $\sigma = 1.82 \times 10^{-3}$ in the supercritical case, and $\sigma = 2.37 \times 10^{-3}$ in the subcritical case. Moreover, we find that in all cases the singularity spectrum is biased to the right side of the maximum value of $f(\alpha)$: $\Delta\alpha_{left} < \Delta\alpha_{right}$. Such a right-biased spectrum with an extended high-α tail is further confirmation that the multifractal structures in the jet are dominated by low-amplitude fluctuations. Lastly, we find that the value of α at which $f(\alpha)$ peaks is higher in the subcritical case than in the supercritical case. This suggests that the subcritical data are less correlated, containing more irregular (fine) structures.

Multifractality can arise from two main sources (Kantelhardt *et al.* 2002): (i) different long-range correlations of the small- and large-scale fluctuations, leading to a regular probability density function (PDF) with finite moments; and (ii) a broad PDF of time series values, such as the Lévy distribution. To determine which source is dominant in the present system, we randomly shuffle the original time series to destroy any long-range correlations, thereby making the data memoryless. Figure 2(e,f) shows that unlike the original data, the shuffled data have a singularity spectrum clustered at $\alpha = 0.5$, indicating that the jet dynamics have degenerated to a white-noise-like state. From this we conclude that the multifractality of the jet arises from different long-range correlations of the small- and large-scale fluctuations. Moreover, singularity spectra from the unforced limit-cycle state show clustering at $\alpha = 0$, which is consistent with periodic data dominated by a single time scale. This demonstrates that the jet loses its multifractality when it bifurcates to a limit cycle at the onset of global instability: a feature that is further explored in § 3.4.

3.3. *Scale-free network topology*

We further analyse the noise-induced dynamics of the jet using complex networks built with the visibility algorithm of Lacasa *et al.* (2008). We use the jet velocity fluctuations $u'(t)$ as input, enabling insights to be gained into the kinetic energy of the system. Each element of the time series $u'_i(t_i)$ indexed by $i = 1, \ldots, N$ represents a node in a network. Two arbitrary elements, (t_a, u'_a) and (t_b, u'_b), are considered linked if $u'_c < u'_b + (u'_a - u'_b)[(t_b - t_c)/(t_b - t_a)]$, where (t_c, u'_c) is any other element between elements (t_a, u'_a) and (t_b, u'_b). After mapping the time series to a network using the adjacency
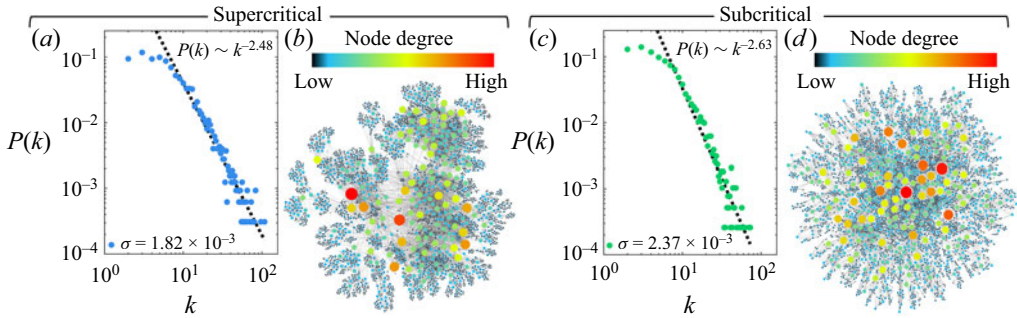
Figure 3. (*a*,*c*) Node degree distribution and (*b*,*d*) network structure for two scale-free cases with strong multifractality: (*a*,*b*) supercritical at $\sigma = 1.82 \times 10^{-3}$ and (*c*,*d*) subcritical at $\sigma = 2.37 \times 10^{-3}$.

matrix **A**, we analyse the network structure using various measures. One such measure is the node degree distribution $P(k)$, which represents the probability distribution of the number of edges k emanating from each node in the network. The node degree distribution is a fundamental property of a complex network, providing insights into its structure and function.

We consider two representative cases: a supercritical case (figure 3*a*,*b*: $\sigma = 1.82 \times 10^{-3}$) and a subcritical case (figure 3*c*,*d*: $\sigma = 2.37 \times 10^{-3}$). Both cases feature strong multifractality, as indicated by the maxima in $\Delta\alpha$ (figure 2*e*,*f*). We find that both types of bifurcation support an inverse power-law scaling in the node degree distribution, $P(k) \sim k^{-\gamma}$ (figure 3*a*,*c*). We use a maximum-likelihood method to estimate $\gamma = 1 + n[\sum_{i=1}^{n} \log(k_i/k_{min})]^{-1}$, where n is the total degrees considered, k_i is the degree itself and k_{min} is the smallest degree for which the power-law scaling holds (here $k_{min} = 6$). We find that $\gamma = 2.48$ and 2.63 for the supercritical and subcritical cases, respectively. Both values are in the range $2 < \gamma < 3$, indicating that both networks exhibit scale-free topology (Barabási & Albert 1999).

The structure of these scale-free networks can be visualised in figure 3(*b*,*d*): for both types of bifurcation, the low-k nodes far outnumber the high-k nodes. The high-k nodes are known as hubs (red/orange circles), occupy the tail end of the power-law distribution, and determine the resiliency of the network (Iacobello *et al.* 2021). In turbulent flows, such hubs could represent large-scale coherent structures, whereas the low-k nodes could represent small-scale vortices generated by the turbulent energy cascade (Murugesan & Sujith 2015; Taira *et al.* 2016). In our globally stable laminar jet, the hubs represent intermittent bursts of periodicity arising from coherence resonance (Zhu *et al.* 2019): the peaks of such bursts provide a clear line-of-sight to other peaks, increasing k. This is the origin of the observed scale-free network topology.

3.4. *Early detection of global instability*

Early warning indicators have been used to forewarn of impending critical transitions in various nonlinear dynamical systems (Scheffer *et al.* 2009). Two such indicators are H_2, as computed via multifractal analysis, and the global clustering coefficient C_g, as computed via network analysis. The indicator C_g was introduced by Watts & Strogatz (1998) to quantify the extent of node clustering in a complex network. It is defined as the number of
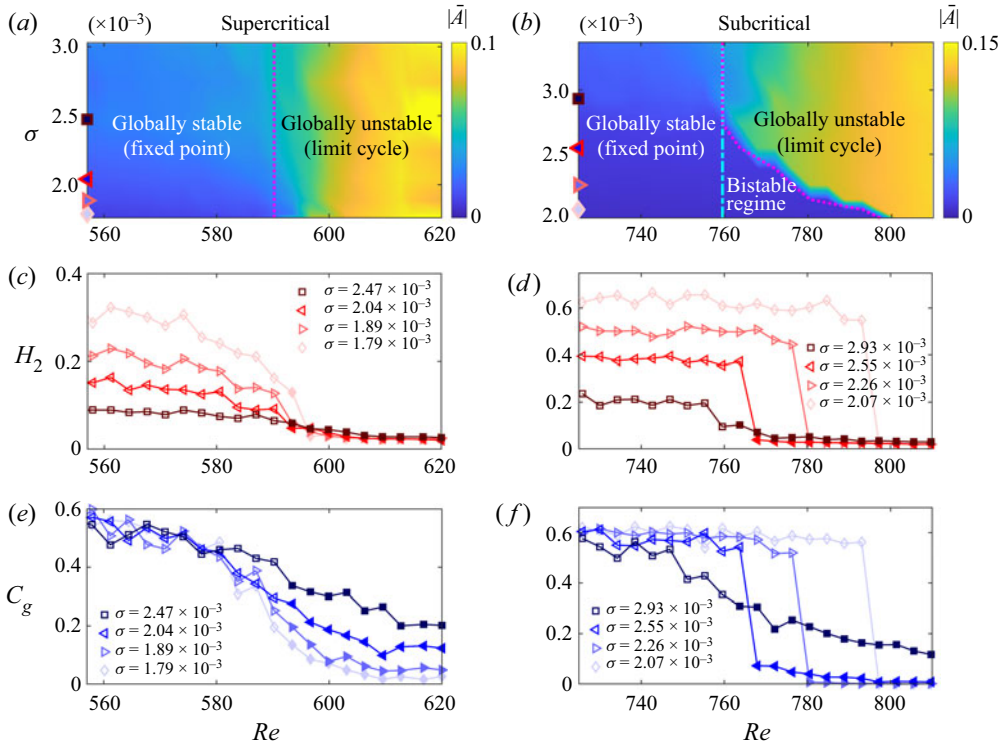
Figure 4. Early detection of global instability: (*a,b*) bifurcation diagrams, (*c,d*) the Hurst exponent H_2, and (*e,f*) the global clustering coefficient C_g, all as functions of Re for different noise intensities σ. In panels (*c–f*), the hollow markers denote globally stable states, while the filled markers denote globally unstable states. The supercritical and subcritical cases are shown in the left and right columns, respectively.

closed triplets normalised by the total number of open and closed triplets:

$$C_g \equiv \frac{1}{N} \sum_{i=1}^{N} \left\{ \left(\sum_{j,k=1}^{N} A_{ij} A_{jk} A_{ki} \right) \bigg/ [k_i (k_i - 1)] \right\}, \tag{3.3}$$

where A_{ij} is an edge in the adjacency matrix $\textbf{\textit{A}}$ and $k_i = \sum_{j=1}^{N} A_{ij}$ is the degree centrality, a measure of the number of edges incident to a given node i. The value of C_g ranges from 0 to 1, with higher values indicating that nodes in the network tend to cluster together more tightly. Figure 4 shows the bifurcation diagrams, H_2 and C_g, all as functions of Re for different values of σ. In the subcritical case (figure 4*b*), the bistable regime shrinks as σ increases owing to noise-induced triggering, eventually disappearing altogether at high σ and making the bifurcation appear supercritical.

First we consider H_2. In the supercritical case (figure 4*c*), H_2 decreases gradually towards zero as Re increases towards the Hopf point, indicating that the mean-reversion processes of the jet become stronger as the onset of global instability is approached. Crucially, the decrease in H_2 occurs well before the jet oscillation amplitude ($|\bar{A}|$) starts to rise. This suggests that it might be possible to estimate the proximity to the supercritical Hopf point based on a calibrated H_2 threshold. Such a threshold, however, would depend on the noise intensity because the rate at which H_2 decreases with Re diminishes as σ increases. Physically this occurs because while the jet is globally stable before the Hopf

point, it is still convectively unstable (Huerre & Monkewitz 1990). Convectively unstable modes tend to spatially amplify any injected noise, at certain frequencies more than others, causing a preferred mode to emerge via coherence resonance (Zhu *et al.* 2019). Thus, somewhat counterintuitively, noise promotes order, enhancing the coherence of the jet and reducing the sensitivity of H_2 to Re. In the subcritical case (figure 4*d*), H_2 remains relatively constant at each σ as Re increases towards the Hopf point, after which H_2 falls sharply. This indicates that H_2 is not a reliable precursor of global instability arising from a subcritical Hopf bifurcation.

Next we consider C_g. In the supercritical case (figure 4*e*), C_g decreases gradually as Re increases towards the Hopf point, making it another potential precursor of global instability. This decrease in C_g is insensitive to σ before the Hopf point. After the Hopf point, C_g levels off as σ increases because strong noise tends to disrupt the intrinsic periodicity of the limit-cycle oscillations, reducing the number of network links and thus increasing C_g in the post-bifurcation regime. In the subcritical case (figure 4*f*), C_g behaves like H_2 (figure 4*d*) in that it remains relatively constant as Re increases towards the Hopf point, making it an ineffective precursor at low to moderate noise intensities. Only when the noise intensity is high enough ($\sigma = 2.93 \times 10^{-3}$) to cause the hysteretic bistable regime to disappear can C_g become a potential precursor.

From these observations, we propose that combining H_2 and C_g, along with their slopes, into an integrated algorithm could lead to a systematic methodology for early detection of global instability. Our analysis shows that in the supercritical case, $\partial H_2/\partial Re$ starts off near zero but decreases as the Hopf point is approached, particularly at low σ (figure 4*c*). At the same time, $\partial C_g/\partial Re$ remains relatively constant at all σ (figure 4*e*). In the subcritical case, $\partial H_2/\partial Re$ remains relatively constant at all σ (figure 4*d*), whereas $\partial C_g/\partial Re$ decreases as σ increases (figure 4*f*). These differences in $\partial H_2/\partial Re$ and $\partial C_g/\partial Re$ could be exploited to identify the bifurcation type. Once the bifurcation type is identified (and σ is measured), H_2 or C_g could be used as an instability precursor in the supercritical case, because both of these indicators decrease as Re approaches the Hopf point, with C_g benefiting from reduced sensitivity to σ. However, a calibration step would be needed to determine the critical values to which H_2 and C_g decrease at the supercritical Hopf point. Meanwhile, C_g could be used as an instability precursor in the subcritical case, but only if σ is high. If σ is not high, neither H_2 nor C_g is effective in the subcritical case. Taken together, these criteria may serve as the foundation of an early detection algorithm that synergistically combines multifractal analysis and complex network analysis.

3.5. *Universal scaling between H_2 and β*

Nearly all early warning indicators of critical transitions rely on extracting information from the noise-induced dynamics of the system (Scheffer *et al.* 2009). Such precursors can be classified into two types: (i) those that quantify the complexity or long-term memory of a time series; and (ii) those that quantify the degree of coherence. Prime examples of the former and latter types are, respectively, H_2 (Hurst 1951) and the coherence factor β (Ushakov *et al.* 2005; Zhu *et al.* 2019). Figure 5 shows that in the globally stable regime of the jet, before the onset of limit-cycle oscillations, an inverse power-law scaling exists between H_2 and β for both supercritical and subcritical Hopf bifurcations. Using least-squares regression, we find that the scaling $H_2 \sim \beta^{-\zeta}$ has a coefficient of determination of $R^2 = 0.92$ with $\zeta = 0.48$ in the supercritical case and $R^2 = 0.82$ with $\zeta = 0.28$ in the subcritical case. These scaling laws are independent of Re and σ, giving them some degree of universality for the early detection of global instability in low-density jets.
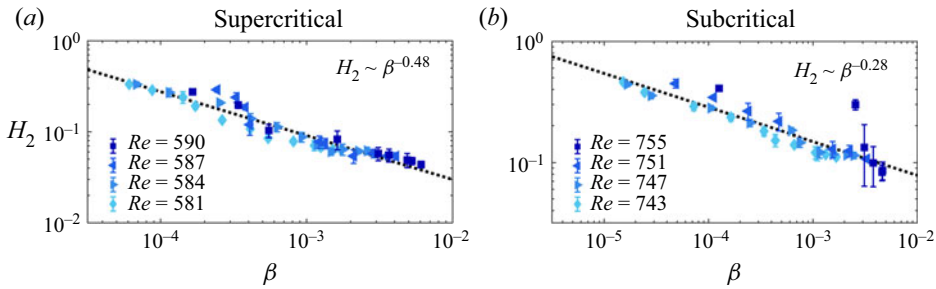
Figure 5. Inverse power-law scaling between H_2 and β for various σ in the globally stable regime, prior to (*a*) supercritical and (*b*) subcritical Hopf bifurcations. The error bars denote the standard deviation of H_2.

4. Conclusions

We have provided the first experimental evidence of multifractality and scale-free network topology in a laminar flow: a noise-perturbed low-density jet operated at a Reynolds number below the critical point of a supercritical Hopf bifurcation and below the saddle-node point of a subcritical Hopf bifurcation. We stochastically forced the jet with acoustic waves of different amplitudes σ and characterised its noise-induced dynamics via multifractal detrended fluctuation analysis and complex network analysis. For both supercritical and subcritical Hopf bifurcations, we found that (i) the degree of multifractality, as quantified by the width of the singularity spectrum, reaches a maximum at intermediate noise intensities; (ii) the conditions with the strongest multifractality give rise to a complex network whose node degree distribution obeys an inverse power-law scaling with an exponent of $2 < \gamma < 3$, indicating scale-free topology; and (iii) the Hurst exponent H_2 and the global clustering coefficient C_g can serve as early warning indicators of global instability, but their effectiveness depends on the bifurcation type and the noise intensity. Specifically, we have found that both H_2 and C_g can serve as precursors of supercritical Hopf bifurcations, especially when σ is low. However, we also found that only C_g can serve as a precursor of subcritical Hopf bifurcations, and only under specific forcing conditions: when σ is high enough to merge the saddle-node and Hopf points, eliminating the hysteretic bistable regime. Finally, we have identified a universal power-law scaling between H_2 and the coherence factor β, establishing a link between fractal-based and coherence-based precursors of global instability.

Although both multifractality and scale-free network topology have previously been observed in turbulent flows, they have not been observed in a laminar flow – until now. Here we have shown that applying stochastic forcing to a laminar flow can cause it to exhibit the same type of multifractal and scale-free network dynamics usually seen in turbulent flows. This discovery supports the notion that the complex dynamics of turbulent flows can be modelled with low-order oscillators subjected to additive noise (Noiray & Schuermans 2013; Rigas *et al.* 2015; Sieber *et al.* 2021). This discovery also supports the notion that deterministic spatiotemporal chaos in hydrodynamic systems can be modelled with the Kardar–Parisi–Zhang (KPZ) equation, a nonlinear stochastic partial differential equation. Many spatiotemporally chaotic systems are known to belong to the KPZ universality class, demonstrating that the small-scale features of deterministic systems can have effects equivalent to those of a stochastic noise term (Boghosian, Chow & Hwa 1999). Further evidence to support this can be found in the shell models used by physicists to understand the complexity of turbulence (Biferale 2003). Shell models lack the spatial structure of turbulence, yet they retain most of the temporal complexity.

These models are dimensionally consistent with the Navier–Stokes equations and can reproduce the multiscale dynamics of three-dimensional turbulence, without incorporating any geometrical complexity (Biferale 2003). Finally, we note that the ability of H_2 and C_g to forewarn of an impending critical transition to global instability could find uses in various other self-excitable flows, such as bluff-body wakes and swirling jets. The applicability of these early warning indicators to such flows remains to be explored.

Declaration of interests. The authors report no conflict of interest.

Author ORCIDs.

Ⓘ Yu Guan https://orcid.org/0000-0003-4454-3333;

Ⓘ Yuanhang Zhu https://orcid.org/0000-0002-2080-1142;

Ⓘ Vikrant Gupta https://orcid.org/0000-0003-3990-9505;

Ⓘ Larry K.B. Li https://orcid.org/0000-0002-0820-170X.

REFERENCES

BARABÁSI, A. & ALBERT, R. 1999 Emergence of scaling in random networks. *Science* **286** (5439), 509–512.

BIFERALE, L. 2003 Shell models of energy cascade in turbulence. *Annu. Rev. Fluid Mech.* **35** (1), 441–468.

BOGHOSIAN, B.M., CHOW, C.C. & HWA, T. 1999 Hydrodynamics of the Kuramoto–Sivashinsky equation in two dimensions. *Phys. Rev. Lett.* **83** (25), 5262.

CHAKRAVARTHY, R.V.K., LESSHAFFT, L. & HUERRE, P. 2018 Global stability of buoyant jets and plumes. *J. Fluid Mech.* **835**, 654–673.

CHOMAZ, J.M., HUERRE, P. & REDEKOPP, L.G. 1988 Bifurcations to local and global modes in spatially developing flows. *Phys. Rev. Lett.* **60** (1), 25.

COENEN, W., LESSHAFFT, L., GARNAUD, X. & SEVILLA, A. 2017 Global instability of low-density jets. *J. Fluid Mech.* **820**, 187–207.

CONIGLIO, A., DE ARCANGELIS, L. & HERRMANN, H. 1989 Fractals and multifractals: applications in physics. *Physica* A **157** (1), 21–30.

FLOHR, P. & OLIVARI, D. 1994 Fractal and multifractal characteristics of a scalar dispersed in a turbulent jet. *Physica* D **76** (1–3), 278–290.

HALLBERG, M.P. & STRYKOWSKI, P.J. 2006 On the universality of global modes in low-density axisymmetric jets. *J. Fluid Mech.* **569**, 493–507.

HUERRE, P. & MONKEWITZ, P.A. 1990 Local and global instabilities in spatially developing flows. *Annu. Rev. Fluid Mech.* **22** (1), 473–537.

HURST, H. 1951 Long-term storage capacity of reservoirs. *Trans. Am. Soc. Civil Engrs* **116** (1), 770–799.

IACOBELLO, G., RIDOLFI, L. & SCARSOGLIO, S. 2021 A review on turbulent and vortical flow analyses via complex networks. *Physica* A **563**, 125476.

IHLEN, E. 2012 Introduction to multifractal detrended fluctuation analysis in Matlab. *Front. Physiol.* **3**, 97.

JHAWAR, J., MORRIS, R., AMITH-KUMAR, U., RAJ, M., ROGERS, T., RAJENDRAN, H. & GUTTAL, V. 2020 Noise-induced schooling of fish. *Nat. Phys.* **16** (4), 488–493.

KANTELHARDT, J. 2012 Fractal and multifractal time series. In *Mathematics of Complexity and Dynamical Systems* (ed. R.A. Meyers), pp. 463–487. Springer.

KANTELHARDT, J., ZSCHIEGNER, S., KOSCIELNY-BUNDE, E., HAVLIN, S., BUNDE, A. & STANLEY, H. 2002 Multifractal detrended fluctuation analysis of nonstationary time series. *Physica* A **316** (1), 87–114.

KUSHWAHA, A.K., WORTH, N.A., DAWSON, J.R., GUPTA, V. & LI, L.K.B. 2022 Asynchronous and synchronous quenching of a globally unstable jet via axisymmetry breaking. *J. Fluid Mech.* **937**, A40.

KYLE, D.M. & SREENIVASAN, K.R. 1993 The instability and breakdown of a round variable-density jet. *J. Fluid Mech.* **249**, 619–664.

LACASA, L., LUQUE, B., BALLESTEROS, F., LUQUE, J. & NUNO, J. 2008 From time series to complex networks: the visibility graph. *PNAS* **105** (13), 4972–4975.

LEE, M., GUAN, Y., GUPTA, V. & LI, L.K.B. 2020 Input-output system identification of a thermoacoustic oscillator near a Hopf bifurcation using only fixed-point data. *Phys. Rev.* E **101** (1), 013102.

LEE, M., KIM, K.T., GUPTA, V. & LI, L.K.B. 2021 System identification and early warning detection of thermoacoustic oscillations in a turbulent combustor using its noise-induced dynamics. *Proc. Combust. Inst.* **38** (4), 6025–6033.

LEE, M., ZHU, Y., LI, L.K.B. & GUPTA, V. 2019 System identification of a low-density jet via its noise-induced dynamics. *J. Fluid Mech.* **862**, 200–215.

LESSHAFFT, L. & MARQUET, O. 2010 Optimal velocity and density profiles for the onset of absolute instability in jets. *J. Fluid Mech.* **662**, 398–408.

LI, L.K.B. & JUNIPER, M.P. 2013*a* Lock-in and quasiperiodicity in a forced hydrodynamically self-excited jet. *J. Fluid Mech.* **726**, 624–655.

LI, L.K.B. & JUNIPER, M.P. 2013*b* Phase trapping and slipping in a forced hydrodynamically self-excited jet. *J. Fluid Mech.* **735** (R5), 1–11.

LINDNER, B., GARCIA-OJALVO, J., NEIMAN, A. & SCHIMANSKY-GEIER, L. 2004 Effects of noise in excitable systems. *Phys. Rep.* **392** (6), 321–424.

LIU, C., ZHOU, W. & YUAN, W. 2010 Statistical properties of visibility graph of energy dissipation rates in three-dimensional fully developed turbulence. *Physica* A **389** (13), 2675–2681.

LÓPEZ, P., TARQUIS, A., MATULKA, A., SKADDEN, B. & REDONDO, J. 2017 Multiscaling properties on sequences of turbulent plumes images. *Chaos, Solitons Fractals* **105**, 128–136.

MENEVEAU, C. & SREENIVASAN, K.R. 1991 The multifractal nature of turbulent energy dissipation. *J. Fluid Mech.* **224**, 429–484.

MURUGESAN, M. & SUJITH, R.I. 2015 Combustion noise is scale-free: transition from scale-free to order at the onset of thermoacoustic instability. *J. Fluid Mech.* **772**, 225–245.

MURUGESAN, M. & SUJITH, R.I. 2016 Detecting the onset of an impending thermoacoustic instability using complex networks. *J. Propul. Power* **32** (3), 707–712.

NAIR, V. & SUJITH, R.I. 2014 Multifractality in combustion noise: predicting an impending combustion instability. *J. Fluid Mech.* **747**, 635–655.

NOIRAY, N. & SCHUERMANS, B. 2013 Deterministic quantities characterizing noise driven Hopf bifurcations in gas turbine combustors. *Intl J. Non-Linear Mech.* **50**, 152–163.

PIKOVSKY, A.S., ROSENBLUM, M.G. & KURTHS, J. 2003 *Synchronization: A Universal Concept in Nonlinear Sciences*. Cambridge University Press.

RIGAS, G., MORGANS, A., BRACKSTON, R. & MORRISON, J. 2015 Diffusive dynamics and stochastic models of turbulent axisymmetric wakes. *J. Fluid Mech.* **778**, R2.

SCHEFFER, M., BASCOMPTE, J., BROCK, W.A., BROVKIN, V., CARPENTER, S.R., DAKOS, V., HELD, H., VAN NES, E.H., RIETKERK, M. & SUGIHARA, G. 2009 Early-warning signals for critical transitions. *Nature* **461** (7260), 53–59.

SIEBER, M., PASCHEREIT, C. & OBERLEITHNER, K. 2021 Stochastic modelling of a noise-driven global instability in a turbulent swirling jet. *J. Fluid Mech.* **916**, A7.

SILCHENKO, A. & HU, C. 2001 Multifractal characterization of stochastic resonance. *Phys. Rev.* E **63** (4), 041105.

SREENIVASAN, K.R. 1991 Fractals and multifractals in fluid turbulence. *Annu. Rev. Fluid Mech.* **23** (1), 539–604.

SUJITH, R.I. & PAWAR, S.A. 2021 *Thermoacoustic Instability: A Complex Systems Perspective*. Springer.

TAIRA, K., NAIR, A. & BRUNTON, S.L. 2016 Network structure of two-dimensional decaying isotropic turbulence. *J. Fluid Mech.* **795**, R2.

TAIRA, K. & NAIR, A.G. 2022 Network-based analysis of fluid flows: progress and outlook. *Prog. Aerosp. Sci.* **131**, 100823.

USHAKOV, O., WÜNSCHE, H., HENNEBERGER, F., KHOVANOV, I., SCHIMANSKY-GEIER, L. & ZAKS, M. 2005 Coherence resonance near a Hopf bifurcation. *Phys. Rev. Lett.* **95** (12), 123903.

VIGGIANO, B., SAKRADSE, G., SMITH, S., MUNGIN, R., RAMASUBRAMANIAN, P., RINGLE, D., TRAVIS, K., ALI, N., SOLOVITZ, S. & CAL, R. 2021 Intermittent event evaluation through a multifractal approach for variable density jets. *Chaos, Solitons Fractals* **146**, 110799.

WATTS, D.J. & STROGATZ, S.H. 1998 Collective dynamics of 'small-world' networks. *Nature* **393** (6684), 440–442.

WILKOWSKI, D., RINGOT, J., HENNEQUIN, D. & GARREAU, J. 2000 Instabilities in a magneto-optical trap: noise-induced dynamics in an atomic system. *Phys. Rev. Lett.* **85** (9), 1839.

ZHU, Y., GUPTA, V. & LI, L.K.B. 2017 Onset of global instability in low-density jets. *J. Fluid Mech.* **828**, R1.

ZHU, Y., GUPTA, V. & LI, L.K.B. 2019 Coherence resonance in low-density jets. *J. Fluid Mech.* **881**, R1.